Three-dimensional Mach-Zehnder interferometer in a microfluidic chip for spatially-resolved label-free detection

Andrea Crespi,[a] Yu Gu,[b] Bongkot Ngamsom,[c] Hugo J. W. M. Hoekstra,[d] Chaitanya Dongre,[d] Markus Pollnau,[d] Roberta Ramponi,[a] Hans H. van den Vlekkert,[e] Paul Watts,[c] Giulio Cerullo[a] and Roberto Osellame*[a]

Received 28th September 2009, Accepted 4th January 2010
First published as an Advance Article on the web 9th February 2010
DOI: 10.1039/b920062b

Ultrafast laser writing of waveguides in glasses is a very flexible and simple method for direct on-chip integration of photonic devices. In this work we present a monolithic optofluidic device in fused silica providing label-free and spatially-resolved sensing in a microfluidic channel. A Mach-Zehnder interferometer is inscribed with the sensing arm orthogonally crossing the microfluidic channel and the reference arm passing over it. The interferometer is integrated either with a microchannel fabricated by femtosecond laser technology or into a commercial lab-on-chip for capillary electrophoresis. The device layout, made possible by the unique three-dimensional capabilities of the technique, enables label-free sensing of samples flowing in the microchannel with spatial resolution of about 10 μm and limit of detection down to 10^{-4} RIU.

1. Introduction

Many different functionalities have already been implemented on a lab-on-a-chip (LOC), however integration of the analysis system is still a challenge.[1] Optical sensing techniques are very powerful and widely employed in LOCs; they are immune from electromagnetic interference, capable of performing non-contact sensing, and can provide multiplexed detection within a single device.[2] Traditionally, optical detection in LOCs is performed using bulk equipment, such as mirrors, prisms, lenses and microscope objectives. Such schemes can provide high sensitivity but they require accurate mechanical alignment of the optics to the microfluidic channels and suffer from mechanical vibrations and drifts. Furthermore, the employment of massive benchtop instrument undermines many of the advantages of the LOC approach. In particular, device portability is strongly limited, hampering in-field and point-of-care applications. Much of the commercial success of the LOC concept will depend on the ability to successfully integrate optical detection schemes, enabling a significant reduction in size, costs and overall complexity of the system. For these reasons, several efforts have been made to integrate guided optic devices to perform on-chip optical detection.[1,3] Use of optical waveguides has many clear advantages with respect to standard free-space detection systems, in terms of alignment precision, compactness and portability.

[a]*Istituto di Fotonica e Nanotecnologie-CNR, Dipartimento di Fisica-Politecnico di Milano, Piazza L. da Vinci, 32, 20133 Milano, Italy. E-mail: roberto.osellame@polimi.it*
[b]*Department of Electrical Engineering and Computer Science and Research Laboratory of Electronics, Massachusetts Institute of Technology (MIT), Cambridge, Massachusetts, 02139, USA*
[c]*Department of Chemistry, University of Hull, Cottingham Road, Hull, HU6 7RX, UK*
[d]*Integrated Optical MicroSystems, MESA+ Institute for Nanotecnology, University of Twente, PO Box 217, 7500, AE Enschede, The Netherlands*
[e]*LioniX BV, PO Box 456, 7500, AL Enschede, The Netherlands*

The most commonly used transduction signals in optical sensing are fluorescence and refractive index. Fluorescence detection, due to its background-free nature, provides the highest sensitivity, down to the single-molecule limit.[4] However, this approach suffers from laborious labeling processes that may interfere with the function of a biomolecule or living cell, or may prevent on-chip chemical reactions from taking place. On the other hand, the measurement of refractive index variations allows label-free sensing, detecting the analyte in its natural form without any alteration. This detection approach is particularly suited for monitoring the kinetics of transient processes without interfering with the reactions.

Various monolithic optical devices for refractive index sensing have been proposed;[5] standard approaches, based on integrated optics, include Mach-Zehnder Interferometers (MZIs),[6] Young interferometers,[7] and Bragg gratings.[8] These devices are fabricated by various techniques including plasma vapour deposition, reactive ion etching, and also liquid-core waveguides.[9] However, all these techniques are only capable of producing two-dimensional optical circuits. In addition, these devices typically exploit interaction between the evanescent field of the guided mode and the fluid in the microchannel, requiring long interaction lengths (millimetres to centimetres) for sensitive detection. On the other hand, several microfluidic applications call for spatially selective label-free detection, *e.g.* when molecules are separated in a microchannel by capillary electrophoresis or when counting is required as in cell flow cytometry. In addition, spatially selective refractive index detection would enable multipoint sensing, *e.g.* for monitoring the reaction kinetics in chemical microreactors.[10]

The integration of optical waveguides or other photonic components with microfluidic channels is not a straightforward process. In fact, it requires a local modification of the refractive index of the substrate, which means adding further lithographic steps, thus complicating the fabrication process of the chip. Recently, a novel technique for the direct writing of waveguides and photonic circuits in glass substrates, exploiting refractive

index modifications induced by focused femtosecond pulses, has emerged.[11,12] Compared with traditional techniques, femtosecond waveguide writing in a glass chip offers two striking advantages: (i) it is a direct maskless fabrication technique, *i.e.* in a single step one can create optical waveguides or more complicated photonic devices (splitters, interferometers, *etc.*) by simply moving the sample with respect to the laser focus; (ii) it is a three-dimensional (3D) technique, since it allows one to define waveguides at arbitrary depths inside the glass. For these reasons, this technique appears highly suited for the integration of optical waveguides into LOCs. In fact, the 3D capabilities allow much more compact layouts and greater freedom in the design. In addition, this technique can be applied to post-processing of LOCs fabricated by standard technologies, enabling a straightforward upgrade of chips that have already been optimized for microfluidic functionality.[13–15] Femtosecond laser technology combined with selective chemical etching can also fabricate directly buried microchannels,[16,17] and thus a single laser system can be used to produce the entire optofluidic device.[18–21]

In this work we present a monolithic device for label-free and spatially-resolved optical sensing in a microfluidic chip. Two possible configurations are explored. In the first one the optofluidic chip is completely fabricated by femtosecond laser technology in a fused silica substrate (layout is shown in Fig. 1). It consists of a microchannel integrated with a MZI having the sensing arm orthogonally crossing the channel and the reference arm passing over it. The device is capable of refractive index sensing with a spatial resolution of the order of the waveguide mode diameter (11 μm). The innovative 3D layout of the MZI, which is required for spatially-resolved sensing, is only made possible by the unique capabilities of femtosecond laser microstructuring. Since this geometry implies a very small interaction length with the analyte, evanescent field sensing would provide a limited sensitivity; therefore, in our configuration, the sensing arm directly intersects the microchannel. The device is statically and dynamically tested by filling the channel with glucose solutions and displays a sensitivity down to 10^{-4} Refractive Index Units (RIU). The second configuration integrates the 3D MZI device in a commercial LOC for capillary electrophoresis. In this case only the MZI is fabricated by femtosecond laser writing, while the fluidic part is produced with conventional technologies in fused silica. Calibration of the optofluidic device is achieved using glucose solutions and measurements of different concentrations of peptides are performed.

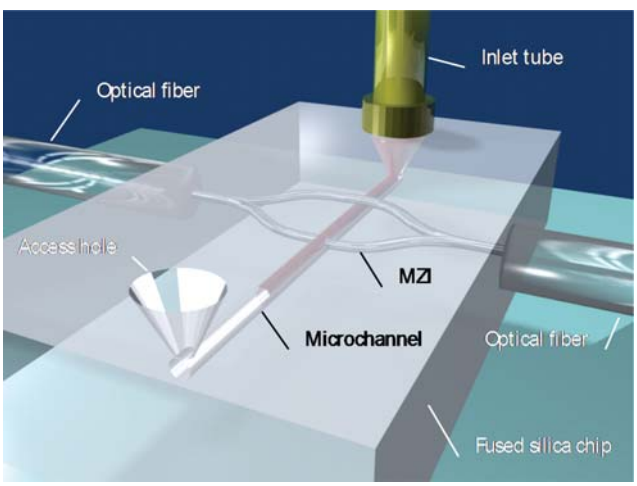

Fig. 1 Schematic of the femtosecond-laser-fabricated microfluidic channel and integrated MZI. The sensing arm crosses orthogonally the channel, while the reference one passes over it.

2. Materials and methods

A. Microchannel fabrication

Microchannel fabrication in fused silica samples (Foctek, China) is performed by irradiation with femtosecond laser pulses followed by etching with a 20% acqueous solution of hydrofluoric acid (HF).[16] A regeneratively amplified Ti:Sapphire laser (150-fs, 5-μJ pulses at 1 kHz and 800 nm) is astigmatically beam shaped and focused by a 0.6 NA objective and irradiates a line along the desired path in the substrate.[17,22]

High-intensity femtosecond laser irradiation in fused silica creates self-ordered nanocracks, orthogonally aligned to the laser polarization.[23] When the sample is immersed in the HF solution, the etchant rapidly diffuses in the nanocracks along the irradiated line and chemically dissolves the surrounding material. This creates high aspect ratio microchannels with nearly circular cross-section and diameters of several tens of micrometres, significantly exceeding the irradiated region, which has a diameter in the order of a few micrometres. Since microchannel diameter grows with etching duration, immersion time is controlled to obtain the desired size. The inner wall roughness of the microchannel is estimated to be less than 500 nm rms, independently from the spot size and the irradiation parameters.

Exploiting the 3D capabilities of this technology, a U-shaped microfluidic channel is fabricated in a single irradiation step (schematic is shown in Fig. 1). Two access holes connect the 2-mm long and 100-μm buried microchannel to the top surface of the sample. The average diameter of the microchannel is about 60 μm and external connection to syringes is achieved by gluing a Luer Lock connector to one of the access holes.

B. Waveguide fabrication

We fabricate optical waveguides in the same fused silica substrate previously used for microchannel fabrication. The irradiation intensity for waveguide writing is much lower than that used for the pre-etching irradiation in the microchannel fabrication, so that a smooth and uniform refractive index change is obtained along the irradiation path.[23] The mechanism inducing permanent refractive index changes in transparent materials by ultrashort laser irradiation is described elsewhere.[12,24] Briefly, the focusing of ultrashort pulses leads to very high peak intensities which induce strongly nonlinear absorption (due to a combination of multiphoton and avalanche ionization processes) spatially confined to a small volume around the focus. This localized energy deposition can create a permanent increase of the refractive index, by a variety of mechanisms such as densification, color center formation and structural modifications. The refractive index change is exploited, by moving the laser focus inside the substrate, to produce light-guiding structures.

Waveguides are written by a mode-locked Yb:KYW laser producing 350-fs pulses at 1030 nm, with energy up to 1 μJ.[25] The

repetition rate was set to 1 MHz and the second harmonic, produced by a lithium triborate crystal, was used since this fabrication wavelength yields smoother waveguides.[26] This laser is preferable to the amplified Ti:Sapphire laser, used for the microchannel fabrication, since it provides waveguides with a higher refractive index contrast, thus allowing smaller curvature radii. Recently, it has been demonstrated that this laser can also be used for microchannel fabrication,[27] so that one can envisage a single laser tool for fabricating the entire device.

The writing beam is focused into the sample by a 50× objective with 0.6 NA, using an average power of 90 mW. The sample is moved at a speed of 100 μm s^{-1} by a three-axis air-bearing stage (Aerotech FiberGlide 3D). Translation of the sample in the three dimensions is obtained with a precision on the order of 100 nm, enabling the fabrication of fully three-dimensional optical devices with arbitrary shape.

The obtained waveguides display a refractive index contrast $\Delta n \sim 5 \times 10^{-3}$, corresponding to a single guided mode at the 1.5 μm wavelength used for the experiments, with 11-μm diameter.

C. Commercial lab-on-a-chip

In addition to the optofluidic device completely fabricated by femtosecond lasers, we also integrate the 3D MZI into a commercial LOC (LioniX bv) for microchip capillary electrophoresis (MCE). The layout of the microchip is shown in Fig. 2. Two microchannels are present according to the classical cross scheme employed in MCE (actually the cross is folded in order to minimize the footprint of the device). The microchannels are fabricated in a fused silica substrate by photolithography followed by wet etching and have a cross-section with 110 μm width and 50 μm depth. In the sealed chip the microchannels are buried at a depth of 500 μm from its surface. Since for MCE applications the optical detection is required at the end of the separation channel, the MZIs are fabricated in the area evidenced by shading in Fig. 2.

3. Results and discussion

A. MZI fabrication and characterization

As a preliminary step to integration with the microfluidic channel, the MZIs are fabricated in a plain fused silica substrate. We chose to design unbalanced interferometers, so that we could detect fringes in the wavelength dependent transmission when scanning a sufficiently large spectral region with a tunable laser. The device is realized using a combination of circular (radius $R = 30$ mm) and straight segments according to the geometry

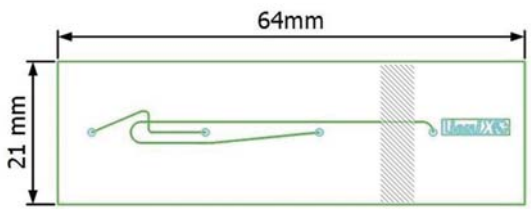

Fig. 2 Schematic of the commercial microchip for capillary electrophoresis (LioniX bv). MZIs will be fabricated in a region at the end of the separation channel indicated by the shaded area.

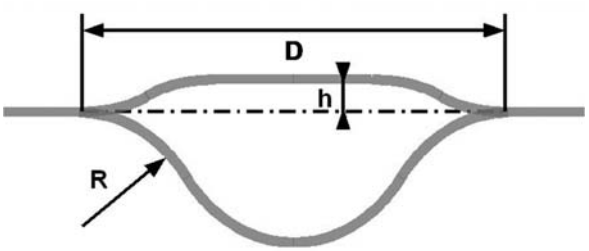

Fig. 3 Schematic of the unbalanced MZI with $h = 50$ μm, $R = 30$ mm and $D = 17$ mm.

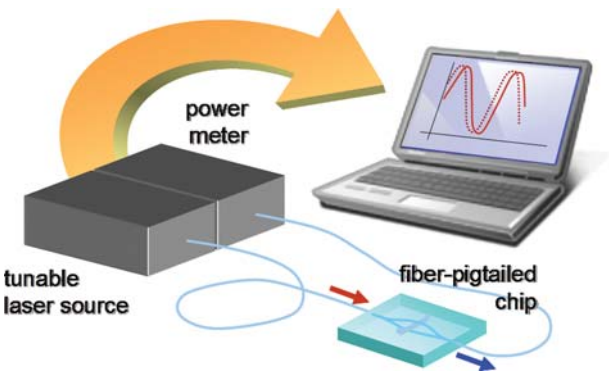

Fig. 4 Schematic of the experimental set-up for measuring the transmission spectrum of the MZI. A tunable laser, fiber pigtailed to the chip, scans the wavelength range of interest. The output power of the MZI is measured at each wavelength by a power meter.

presented in Fig. 3. The unbalance Δs between the two arm lengths is 56 μm. The length of the device is $D = 17$ mm.

Differently from femtosecond laser written MZI devices reported in the literature,[28] the splitter and combiner employ symmetric Y-junctions instead of directional couplers. This increases the compactness of the device and avoids any wavelength dependence of the splitting ratio.

A fiber-coupled tunable laser (Agilent 8164B) emitting 100 μW is used to measure the wavelength dependent transmission of the device from 1460 nm to 1570 nm (the set-up is schematically shown in Fig. 4). The power meter, synchronized with the laser scan, is a module hosted together with the laser in the same instrument. This wavelength range is chosen due to the large availability of compact, widely tunable and stable laser sources. Theory predicts, for an unbalanced interferometer, a power transmission T as a function of wavelength λ expressed by

$$T = \frac{1}{2}\left[1 + \cos\left(\frac{2\pi}{\lambda} n_0 \Delta s\right)\right] \quad (1)$$

where n_0 is the effective refractive index of the guided mode ($n_0 \approx 1.45$ in our fused silica waveguides). Fig. 5 shows the transmission spectrum of the unbalanced MZI together with a fitting curve following the expression in eqn (1). From the fitting function one obtains $\Delta s = 54$ μm which is in very good agreement with the design value $\Delta s = 56$ μm. This demonstrates a remarkable control of the geometric properties of the MZI and of the refractive index uniformity in the two arms. The overall insertion loss of the device, measured after butt-coupling two single-mode fibers at the input and output ports, is 7.4 dB. The fringe visibility

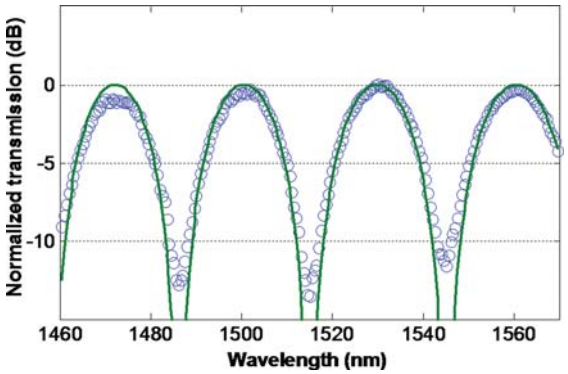

Fig. 5 Open circles: measured transmission spectrum of the MZI. Solid line: least-squares fit of the experimental data.

depends on the splitting ratios of the input and output Y-coupler and on the propagation losses of the guided mode in the interferometer arms.[29] Therefore, the high fringe contrast obtained in our experiment (up to 13 dB in the considered 110 nm spectral range), is a clear indication of the high symmetry in the splitter and combiner sections and of the closely balanced propagation losses in the two arms.

B. Integration of a MZI with a fs-laser fabricated microchannel

Unbalanced MZIs are inscribed in a fused silica chip where a microfluidic channel has been already fabricated by femtosecond laser according to the procedure described in 2A (see schematic in Fig. 1). The shape and the dimensions of the MZI are the same as those described in section 3A. The 90° intersection is chosen in order to achieve spatially selective detection. This high spatial resolution is obtained at the expense of the sensing length, which is limited by the channel width. Therefore, to maximize the phase shift induced by the analyte, direct

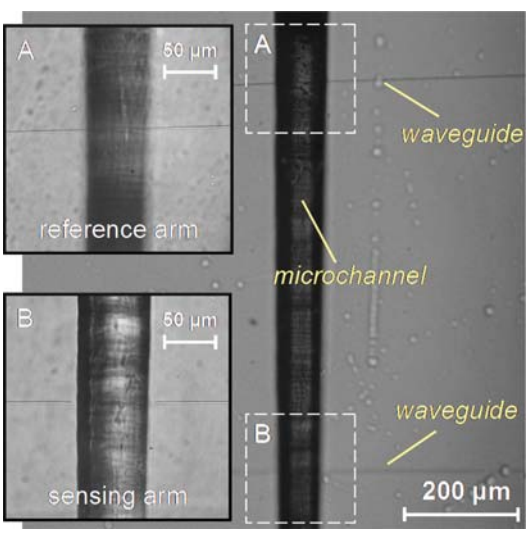

Fig. 6 Microscope picture showing the two arms of the MZI crossing the microfluidic channel. Because of the tilted geometry, the reference arm (panel A) passes over the channel while the sensing arm (panel B) crosses the channel.

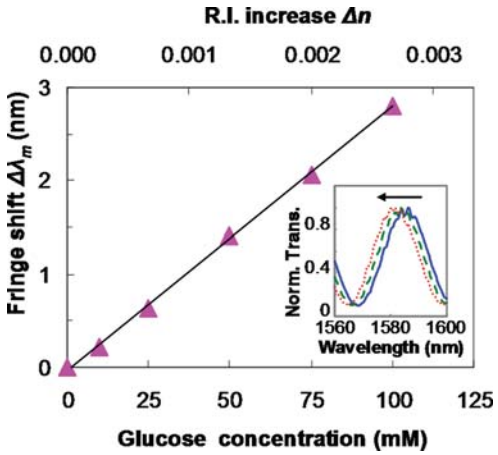

Fig. 7 Measured fringe shift for different concentrations of glucose-D in water (inset: 0 mM solid; 50 mM dashed; 100 mM dotted); the correspondent refractive index increase is also shown in the top axis.

intersection of the sensing arm with the microchannel is chosen. In this way the sensing region is a cylinder with a height equal to the channel diameter (~60 μm) and a base with a diameter of ~15 μm, approximately equal to the waveguide mode size. To enable only one arm intersecting the microchannel, the MZI was inscribed in a plane tilted by 7° with respect to the horizontal. The sensing arm of the MZI (which is chosen as the shorter one) orthogonally intersects the microchannel in its center (see Fig. 6, panel B), while the reference arm passes 20 μm above the microchannel (see Fig. 6, panel A).

To avoid damaging the channel walls, the writing laser beam is blocked with a synchronized shutter while inscribing the sensing arm through the channel. The optical waveguide stops at a distance of ~5 μm from the microchannel wall. The MZI sensing arm, crossing the microchannel filled with water, experiences an additional loss of about 3 dB, due to both scattering at the channel walls and lack of waveguide confinement across the channel. This loss does not significantly affect the device performance, still allowing fringe contrast as high as 10 dB (see inset of Fig. 7).

Note that this tilted geometry of the MZI is necessary to achieve spatially selective sensing, since only one arm has to cross the channel. This is a clear example of an application where the 3D capabilities of femtosecond laser microfabrication are needed. In fact, it would have been very difficult to obtain this geometry with standard integrated optics technologies, which are intrinsically planar.

C. Operation principles of the interferometric sensor

The transmission spectrum of the MZI crossing the microchannel has the following expression, slightly different from eqn (1),

$$T = \frac{1}{2}\left[1 + \cos\left(\frac{2\pi}{\lambda}\left(n_0\Delta s - (n_{channel} - n_0)L\right)\right)\right] \qquad (2)$$

where we have neglected the difference in propagation loss of the two arms, for simplicity. In particular, the phase difference between the two arms of the MZI is not only due to a length

difference (the $n_0\Delta s$ term), but also to a different refractive index of the content of the microchannel ($n_{channel}$) with respect to the effective index of the guided mode (n_0) in the reference arm (the $(n_{channel} - n_0)L$ term, where L is the microchannel width). Consequently, the transmission spectrum shows fringes with peaks positioned at

$$\lambda_m = \frac{n_0\Delta s - (n_{channel} - n_0)L}{m} \quad (3)$$

where m is the fringe order.

If the content of the microchannel changes its refractive index by a quantity Δn, the transmission peaks will shift by

$$\Delta\lambda_m = -\frac{\Delta n \cdot L}{m} \quad (4)$$

Considering a limited portion of the transmission spectrum with m large enough (in our case on the order of 50) we can assume the $\Delta\lambda_m$ shift constant for all the fringes. As a consequence, the shift in the fringe peaks is proportional to the refractive index change Δn in the microchannel.

The fringe shift $\Delta\lambda_m$ can be accurately retrieved by a Fourier transform (FT) of the MZI transmission spectrum. In fact, the FT of the shifted $T(\lambda)$ can be expressed as

$$\mathscr{F}\{T(\lambda - \Delta\lambda_m)\} = \mathscr{F}\{T(\lambda)\}\exp(i\,2\pi\,\Delta\lambda_m f) \quad (5)$$

where f is the Fourier frequency. Monitoring the phase shift of the FT at a fixed frequency f (typically chosen as that corresponding to the peak of the FT amplitude) it is possible to easily retrieve the fringe shift $\Delta\lambda_m$. This procedure can be rapidly and automatically performed by standard numerical methods. It is worth noting that the phase shift $\Delta\phi = 2\pi\,\Delta\lambda_m f$ acquired by the FT, when the transmission spectrum translates by $\Delta\lambda_m$, can be shown to be equal to the phase shift acquired by the light in the sensing arm $\Delta\phi = 2\pi/\lambda\,\Delta n\,L$, when crossing the microchannel with a refractive index variation Δn.

Acquisition of device transmission spectra, using a tunable laser, requires a finite time and is thus particularly suited for static measurements. Many applications, such as capillary electrophoresis, involve the detection of transient signals, requiring faster acquisition times. A different approach, enabling much higher temporal resolution, consists in monitoring the device transmission at a fixed wavelength, where the fringe shift, induced by a refractive index change of the analyte, translates to a change in transmission.

D. Test with glucose solutions

To characterize the sensitivity and the linearity of the interferometer response, the microchannel is filled with different concentrations of acqueous glucose-D solutions, and for each of them the spectral response of the optofluidic device is measured whilst static (see inset in Fig. 7). Fig. 7 shows the fringe shift obtained from the Fourier transform of the measured transmission spectrum as a function of glucose concentration. X-axis top scale represents the corresponding refractive index variation of the solutions with respect to pure water, based on data reported in the literature.[30]

The fringe shift dependence on the molar concentration of the analyte in the microchannel is estimated by a linear fit and is determined to be 28.4 nm M^{-1}. Since the refractive index variation dependence on concentration is known to be 2.66×10^{-2} RIU/M,[30] the device responsivity is estimated at 1070 nm/RIU.

The standard deviation of the data taken from repeated measurements is $\sigma \approx 3 \times 10^{-5}$ RIU, therefore we can extrapolate a limit of detection of 1×10^{-4} RIU with a signal-to-noise ratio ≈ 3. Temperature fluctuations of the analyte (± 0.5 °C) are the limiting factor for device sensitivity, causing most of the noise in index measurements. In fact, the refractive index variation of water due to temperature is on the order of 10^{-4} RIU/ °C. On the other hand, the device in itself is quite insensitive to temperature fluctuations; in fact, the thermo-optical coefficient of fused silica is rather low (10^{-5} RIU/ °C) and temperature-induced index changes of the fused silica waveguides are compensated in the MZI geometry, apart from the relatively small length difference between the two arms.

The intrinsic device sensitivity was assessed by measuring the response with an empty microchannel. In this way, refractive index variations due to sample temperature fluctuations are minimized since the temperature dependence of the refractive index of air is much weaker than that of water. From repeated measurements at room temperature, the RMS noise level is estimated to be $\sigma \approx 3 \times 10^{-6}$ RIU. We thus conclude that the fluctuations in the data of Fig. 7 do not correspond, for the most part, to a noise induced by the instrument or by the data processing technique, but are indeed real variations of the refractive index of the analyte due to temperature fluctuations. Therefore, an order of magnitude improvement in sensitivity could be achieved if the analyte were temperature stabilized.

As discussed in the previous section, in several applications it is important to follow transient signals. A detection approach which consists of monitoring the power at a fixed wavelength is necessary to measure rapidly time-varying signals. At a fixed wavelength, the spectral fringe shift corresponds to a variation in the transmission value. To maximize the sensitivity, the detection wavelength is chosen at an inflection point of the transmission curve.

The same tunable laser used in spectral acquisition is now operated at constant wavelength, and the transmission is acquired *via* a photodetector at 200 ms intervals. A transient measurement is performed by driving the flow of a glucose solution with 30 mM concentration into the channel, which is initially filled with water. A syringe connected to the microchannel is used to apply a constant pressure of 2.2×10^5 Pa, inducing a flow rate of 3 μL s^{-1}. Fig. 8 shows the transition between pure water and the glucose solution, occurring in 2 s. This demonstrates the capability of our device of monitoring fast refractive index transients in the microchannel.

E. Integration of MZIs in a commercial LOC

After demonstrating the proof of concept of spatially-selective label-free sensing in an optofluidic chip completely fabricated by femtosecond laser micromachining, a further step toward application of our approach to LOC devices is performed by integrating a MZI in the commercial LOC described in section 2C. Fig. 9(a) shows four MZIs, fabricated with the same layout detailed in section 3A, at the end of one channel (see shaded area in Fig. 2). Also in this case the sensing arm is crossing the

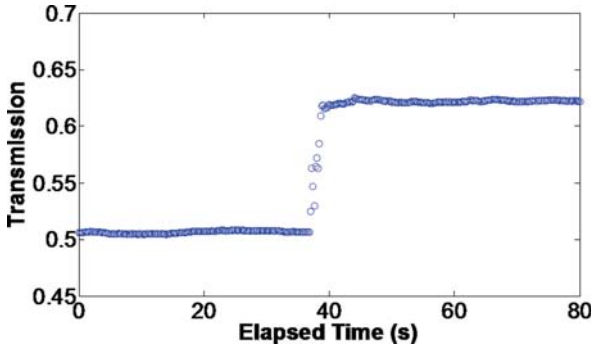

Fig. 8 Transient measurement performed by driving a flow of glucose solution with 30 mM concentration into a channel originally filled with water.

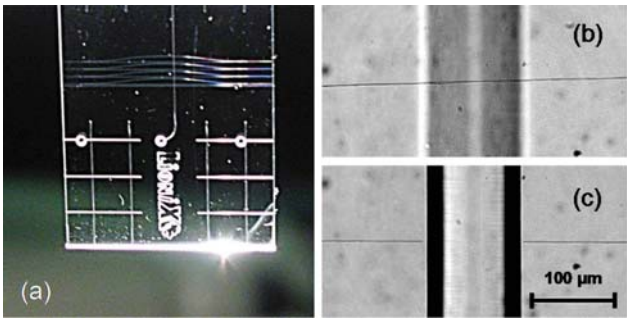

Fig. 9 (a) Picture of the commercial LOC with 4 MZIs inscribed across a microchannel; the grid of microchannels at the bottom of the chip facilitates the sealing of the device and has no fluidic function. Microscope images of (b) the reference arm passing over the microchannel and (c) the sensing arm crossing it.

microchannel, while the reference arm is passing above it (Fig. 9(b) and (c)). Measurements are performed with the same set-up reported in Fig. 4, pigtailing optical fibers to the input and output of one MZI. The high-quality dicing procedure employed by LioniX to sever the different chips in the wafer provides side facets with a sufficient quality to allow coupling the fibers to the waveguides without further polishing.

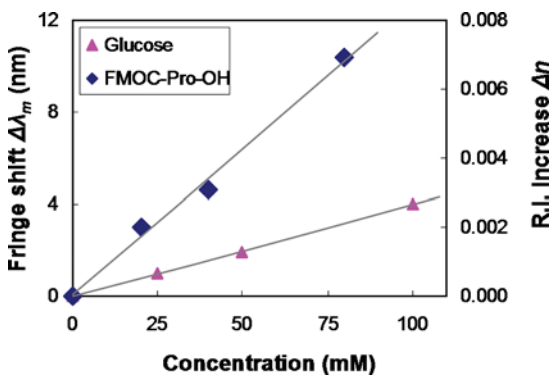

Fig. 10 Measured fringe shift for different concentrations of FMOC-Pro-OH in ethanol (diamonds) and correspondent refractive index increase. The refractive index scale has been calibrated with the data related to glucose in water (triangles).

Sensitivity characterization and device calibration are performed by filling the chip with aqueous glucose-D solutions at different concentrations. Fig. 10 shows the fringe shift calculated from the experimental data, as a function of the glucose concentration. From these measurements the device responsivity is estimated to be 1500 nm/RIU, larger than the one of the device presented in section 3D. The reason for the increased responsivity is the larger width of the microchannel (increased from 60 to 110 μm), thus implying a greater interaction length of light with the fluidic sample (as inferred from eqn (4) the responsivity does not scale linearly with the interaction length L because also m increases with L, see also eqn (3)). Repeating the measurement several times at each concentration a standard error $\sigma \approx 4.8 \times 10^{-5}$ RIU is estimated, which is very similar to that obtained in section 3D. This allows to extrapolate also for this device a limit of detection of $\sim 1.5 \times 10^{-4}$ RIU (equivalent to about 5 mM of glucose-D) for a signal-to-noise ratio SNR = 3.

Having assessed the performance of the device, we have used it to detect biochemically relevant molecules such as peptides, used for drug synthesis in the pharmaceutical industry. Fig. 10 shows the concentration dependent signal of the monopeptide FMOC-Pro-OH in ethanol. The previous calibration, based on glucose solutions, quantitatively associates a refractive index increase to the measured phase shift. Thus, the refractive index dependence on concentration for FMOC-Pro-OH can be determined, and results to be linear with a slope of 8.2×10^{-5} RIU/mM. In this case, given the higher temperature dependence of the refractive index of ethanol with respect to that of water, a standard error of 2.6×10^{-4} RIU is measured. Therefore, we can estimate a limit of detection of 9 mM for the peptides. This value is very well suited for MCE assays of the products of chemical reactions, which are typically in the tens of mM range, and that can be thus monitored in a label-free way thanks to the integrated MZI.

4. Conclusions

A compact and highly integrated interferometric device has been demonstrated, which allows refractive index sensing of the content of a microfluidic channel. The specific device geometry enables measurements with high spatial resolution. The device was tested with glucose solutions, determining a sensitivity of 1×10^{-4} RIU that corresponds to a limit of detection of 4 mM. However, it should be noted that the above sensitivity is mainly limited by temperature fluctuations of the analyte, while the intrinsic sensitivity, measured with an empty channel, is one order of magnitude better.

The combination of label-free sensing and high spatial resolution is uniquely enabled by the femtosecond laser writing technique, which allows the fabrication of a 3D interferometer in which only one arm crosses the microchannel. An additional advantage of our technique is the possibility of integrating photonic devices in microfluidic chips, fabricated by standard techniques, without affecting their manufacturing process. To prove this point, an MZI has been fabricated in a commercial lab-on-a-chip for capillary electrophoresis and several concentrations of a monopeptide have been detected. A limit of detection of ~10 mM for the peptide has been demonstrated which makes the device well suited for assaying the products of chemical reactions. Work is in progress to integrate this device in

a microreactor for monitoring the efficiency of chemical synthesis.

Acknowledgements

This work was supported by the European Commission, FP6 Project Contract No. IST-2005-034562 [Hybrid Integrated Biophotonic Sensors Created by Ultrafast Laser Systems (HIBISCUS)]. Yu Gu acknowledges the Roberto Rocca Project.

References

1 E. Verpoorte, *Lab Chip*, 2003, **3**, 42N–52N.
2 X. Fan, I. White, S. Shopova, H. Zhu, J. Suter and Y. Sun, *Anal. Chim. Acta*, 2008, **620**, 8–26.
3 H. C. Hunt and J. S. Wilkinson, *Microfluid. Nanofluid.*, 2008, **4**, 53–79.
4 H. T. Li, L. M. Ying, J. J. Green, S. Balasubramanian and D. Klenerman, *Anal. Chem.*, 2003, **75**, 1664–1670.
5 P. Dumais, C. L. Callender, J. P. Noad and C. J. Ledderhof, *IEEE Sens. J.*, 2008, **8**, 457–464.
6 R. G. Heideman and P. V. Lambeck, *Sens. Actuators, B*, 1999, **61**, 100–127.
7 A. Ymeti, J. Greve, P. V. Lambeck, T. Wink, S. W. F. M. v. Hovell, T. A. M. Beumer, R. R. Wijn, R. G. Heideman, V. Subramaniam and J. S. Kanger, *Nano Lett.*, 2007, **7**, 394–397.
8 A. S. Jugessur, J. Dou, J. S. Aitchison, R. M. De La Rue and M. Gnan, *Microelectron. Eng.*, 2009, **86**, 1488–1490.
9 D. Yin, E. J. Lunt, M. I. Rudenko, D. W. Deamer, A. R. Hawkins and H. Schmidt, *Lab Chip*, 2007, **7**, 1171–1175.
10 S. J. Haswell, R. J. Middleton, B. O'Sullivan, V. Skelton, P. Watts and P. Styring, *Chem. Commun.*, 2001, 391–398.
11 K. Itoh, W. Watanabe, S. Nolte and C. B. Schaffer, *MRS Bulletin*, 2006, **31**, 620–625.
12 R. R. Gatass and E. Mazur, *Nat. Photonics*, 2008, **2**, 219–225.
13 C. Dongre, R. Dekker, H. J. W. M. Hoekstra, M. Pollnau, R. Martinez-Vazquez, R. Osellame, G. Cerullo, R. Ramponi, R. van Weeghel, G. A. J. Besselink and H. H. van den Vlekkert, *Opt. Lett.*, 2008, **33**, 2503–2505.
14 R. Martinez Vazquez, R. Osellame, M. Cretich, M. Chiari, C. Dongre, H. Hoekstra, M. Pollnau, H. Van den Vlekkert, R. Ramponi and G. Cerullo, *Anal. Bioanal. Chem.*, 2009, **393**, 1209–1216.
15 R. Martinez Vazquez, R. Osellame, D. Nolli, C. Dongre, H. van den Vlekkert, R. Ramponi, M. Pollnau and Giulio Cerullo, *Lab Chip*, 2009, **9**, 91–96.
16 A. Marcinkevicius, S. Juodkazis, M. Watanabe, M. Miwa, S. Matsuo, H. Misawa and J. Nishii, *Opt. Lett.*, 2001, **26**, 277–279.
17 V. Maselli, R. Osellame, G. Cerullo, R. Ramponi, P. Laporta, L. Magagnin and P. L. Cavallotti, *Appl. Phys. Lett.*, 2006, **88**, 191107.
18 R. Osellame, V. Maselli, R. Martinez Vazquez, R. Ramponi and G. Cerullo, *Appl. Phys. Lett.*, 2007, **90**, 231118.
19 M. Kim, D. J. Hwang, H. Jeon, K. Hiromatsu and C. P. Grigoropoulos, *Lab Chip*, 2009, **9**, 311–318.
20 V. Maselli, J. R. Grenier, S. Ho and P. R. Herman, *Opt. Express*, 2009, **17**, 11719–11729.
21 R. Martinez Vazquez, R. Osellame, A. Crespi, C. Dongre, H. Hoekstra, M. Pollnau, H. van den Vlekkert, R. van Weeghel, P. Watts, R. Ramponi and G. Cerullo, *Proc. SPIE*, 2009, **7203**, 720313.
22 K. C. Vishnubhatla, J. Clark, G. Lanzani, R. Ramponi, R. Osellame and T. Virgili, *Appl. Phys. Lett.*, 2009, **94**, 041123.
23 R. Taylor, C. Hnatovsky and E. Simova, *Laser Photonics Rev.*, 2008, **2**, 26–46.
24 D. M. Krol, *J. Non-Cryst. Solids*, 2008, **354**, 416–424.
25 A. Killi, U. Morgner, M. J. Lederer and D. Kopf, *Opt. Lett.*, 2004, **29**, 1288–1290.
26 L. Shah, A. Y. Arai, S. M. Eaton and P. R. Herman, *Opt. Express*, 2005, **13**, 1999–2006.
27 K. C. Vishnubhatla, N. Bellini, R. Ramponi, G. Cerullo and R. Osellame, *Opt. Express*, 2009, **17**, 8685–8695.
28 C. Florea and K. Winick, *J. Lightwave Technol.*, 2003, **21**, 246–253.
29 J. Hong, J. S. Choi, G. Han, J. K. Kang, C.-M. Kim, T. S. Kim and D. S. Yoon, *Anal. Chim. Acta*, 2006, **573–574**, 97–103.
30 R. C. West, Editor, *Handbook of chemistry and physics*, 1983, CRC Press, Boca Raton (USA).